BACHELOR

Time resolved all optical switching with an external field

measuring predictions from the Microscopic Three Temperature Model for different laser fluences

van Haren, Cas

Award date:
2019

Time resolved all optical switching with an external field

Measuring predictions from the Microscopic Three Temperature Model for different laser fluences

Cas van Haren
Supervisors:
prof. dr. B. Koopmans
ir. M.J.G. Peeters

Eindhoven University of Technology
Physics of Nanostructures
May 2019

Abstract

Due to the potential of all-optical switching (AOS) as a technique to write magnetic domains, understanding it is of high importance. To do this, models have been made including the Microscopic Three Temperature Model (M3TM). In this report, an attempt will be made to observe predictions from the M3TM in regards to the effect of the laser fluence on the dynamics of AOS with an external magnetic field. This is done by first optimizing the switched spot size for a range of different laser fluences and then using this range to do time resolved measurements of AOS for an external magnetic field of 100mT. By comparing the data to the predictions a discrepancy can be found which could be explained by slightly altering the M3TM.

Contents

1 Introduction

As the world becomes more reliant on computers and data processing, storage of data becomes ever more important. For the past decades, hard disk drives (HDDs) that used magnetic domains to encode for ones and zeros have been the main storage device. However, the speed at which these magnetic domains can be written is limited[1], and solid state drives that use capacitors to write data more quickly have started taking over. From this trend, it is obvious that data writing speed is paramount and innovations that can increase this speed are therefore of incredible significance. One of these techniques is all optical switching (AOS), a technique that uses femtosecond light pulses to switch the magnetization of a material. Since HDDs show that magnetization can be used to encode bits, it seems likely that AOS could be used to write data. With this, an increase in writing speed of up to 3 orders of magnitude can be realized [2]. In addition to this, the energy consumption per bit written also decreases by a factor of 10[3, 4]. Therefore, all optical switching has the potential to revolutionize the market for cheap data storage.

The first magnetization dynamics on picosecond time scale were discovered in 1996 [5]. Here a sample of Ni was demagnetized within picoseconds via a femtosecond laser pulse as seen in Figure 1.1. Following this, a new research area was created, ultrafast magnetization dynamics. A lot of research went into it, since faster magnetization manipulation could for example be used for faster HDDs. Unexpectedly, AOS was observed in 2007 [6]. In this experiment a GdFeCo alloy was used, and due to the demagnetization dynamics of the Gd and FeCo which will be explained in detail later, the magnetization of the material switched. After this, interest increased even further, since practical purposes were easy to find. The understanding of the process increased, it was for example found that instead of alloys, multilayers of different materials could also be used for AOS. In addition, multiple

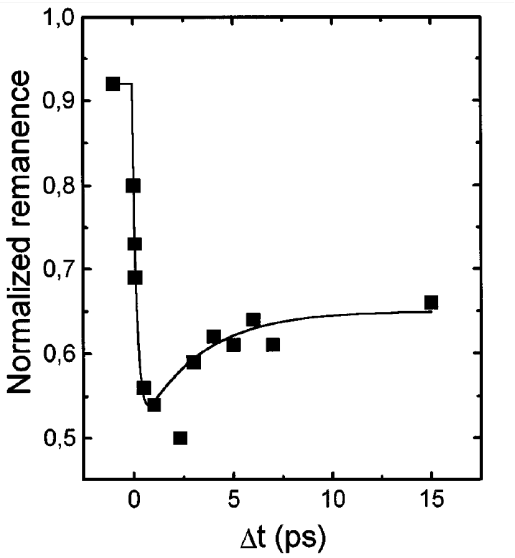

Figure 1.1: Remanence of the magnetization of Nickel after excitation with a 60fs laser pulse. Figure courtesy of Beaurepaire et al.[5]

models were developed to describe and predict the dynamics of AOS. Some of them have shown the ability to correctly predict unobserved phenomena. One of these models is the Microscopic Three Temperature Model (M3TM), based on older models and pioneered in 2005 [7], and improved upon many times since [8, 9, 10, 11].

What is interesting is that there are still predictions made by the model that have not been observed yet. For example, according to the model, the switching for the multilayer structures arises at the interface between the antiferromagnetically coupled layers. Also, the model predicts three different dynamics when a laser pulse hits a multilayer sample with an external field applied depending on the power of the laser pulse. The first dynamic is where the laser pulse is not strong enough, and the material is only demagnetized a little. The second is where the laser pulse is strong enough to switch the material. The third dynamic is where the laser pulse is so strong that the material does not switch anymore. Only the first two of these dynamics have been observed, while the third one might not have been observed due to the laser not being powerful enough.

In this report, an attempt is made to observe this third dynamic. This is done by first optimizing the laser power, which allows for measurements

with a broad range of laser powers. By measuring with these different laser powers, all predicted dynamics should become visible. Searching for these unobserved dynamics predicted by the model can help the model by showing where there are still improvements that can be made.

1.1 Report outline

Chapter 2 explains the historical background of ultrafast magnetization dynamics in detail. All the discoveries that are relevant for this project will be explained. After this the M3TM model will be explained conceptually. Then chapter 3, Methodology, will start by explaining the sample fabrication, sputter deposition. Then the Magneto Optical Kerr Effect (MOKE) setup which allows for the measurement of magnetization will be explained in depth. Following this, the time resolved MOKE (TR-MOKE) setup will be elaborated on. Lastly, the alignment process of the setup in addition to some measurements that demonstrate that earlier results can be reproduced is shown. In chapter 4 the results of all the measurements will be shown and discussed. It will start off with showing the predictions made by the M3TM for AOS with an external field and different laser fluences. It then continues by explaining how a large laser fluence range can be used to measure time resolved switching. After this, measurements for different laser fluences are done to attempt to see the three different mechanisms predicted by the M3TM and a change to the M3TM is proposed based on these results. Chapter 5, Conclusion, will contain a summary of the most relevant measurements. In addition, the change to the M3TM is discussed briefly. In the last chapter, Outlook, new research ideas are suggested that could verify or invalidate the proposed change to the M3TM.

2 Theory

In this chapter the concept of magnetism and the origins of ferromagnetism, antiferromagnetism and ferrimagnetism will be explained. Then, a history of ultrafast magnetization dynamics is given. The history is limited to parts that are relevant for this research project. This includes the first measurements of ultrafast demagnetization, the first measurements of all-optical switching and the first measurements and theory on heat induced all-optical switching. In addition, the M3TM model is explained briefly.

2.1 Magnetism

Magnetism is in its most basic form one aspect of the electromagnetic force created by moving charges. The most familiar form of this effect is caused by ferromagnetic materials. These are materials that can have a permanent magnetization which allow them to attract other ferromagnetic materials without the need of a current to create a magnetic field. The reason for this is that electrons of this material have a magnetic dipole moment caused by their spin, that can be up or down[12]. For most atoms, all the magnetic dipoles of the electrons cancel each other out, causing the atom not to have a magnetic moment. However, when atoms have an uneven number of electrons, this can not be the case and atoms will have a magnetic moment. In some cases, these magnetic moments of nearby atoms tend to align themselves in the same direction due to exchange interaction, which creates large domains with magnetic moments pointing in the same direction. If an external field is then applied, all these domains will start pointing in the same direction of the field. When the field is then removed, and the exchange interaction between the atoms is strong enough, the domains will stay pointing in the same direction. The ferromagnetic material has then become perma-

nently magnetized. There is also another class of magnetic materials called anti-ferromagnetic materials. In these materials, the exchange interaction that caused nearby magnetic moments to align them in the same direction within ferromagnetic materials now instead causes them to align in opposite directions. Because of this, the total magnetization of these materials will be 0, since the magnetic moments of nearby atoms will cancel each other out. If the material consists of different atoms that couple anti-ferromagnetically with each other where one of the atoms has a stronger magnetic moment, a permanent magnetization can still arise, since the magnetic moment of one of the atoms is not completely cancelled out by the other magnetic moment[13], this is called a ferrimagnet.

2.2 Ultrafast Demagnetization

In 1996 Beaurepaire *et al.* showed that ultrafast laser pulses of 50 femtoseconds could demagnetize nickel within 1 picosecond [5]. The reason for this is that the laser first increases the electron temperature, T_{e}, which then heats up the phonon temperature, T_{p}, and the spin temperature, T_{s}. The rapid increase of T_{s} then causes the material to demagnetize. The time evolution of the temperatures can be seen in Figure 2.1. There had been multiple previous experiments done which had not seen this effect [14, 15], but these experiments were done with picosecond laser pulses. This meant that all the three temperatures would stay in equilibrium, and therefore the demagnetization happened on a longer timescale. While demagnetization itself was not extremely relevant yet for any applications, it did show that magnetization dynamics happened at ps time scales, which is multiple orders of magntitude faster than what was previously thought. Because of the relevance of the speed of magnetization dynamics for for example data storage, a substantial amount of research [16, 17, 18] was put into understanding exactly how this demagnetization worked.

2.3 All-Optical Switching

The area of ultrafast demagnetization dynamics became really interesting when the complete switching of magnetization by a light pulse was shown. This was done by Stanciu *et al.* with circularly polarized light. The idea was

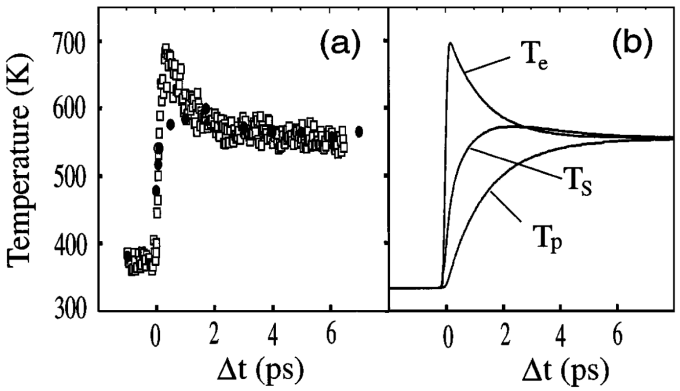

Figure 2.1: Time evolution of the three temperatures baths after laser excitation. A) shows a measurement of the spin and electron temperatures with circles and cubes respectively. B) shows the time evolution according to a model. Figure courtesy of Beaurepaire [5]

that the light would cause the material to demagnetize as shown before and then a magnetic field could be used to switch the magnetization so that when the material cools back down, it re-magnetizes in the other direction. It had recently been shown that circularly polarized light could create a magnetic field within a material via the inverse Faraday effect[19]. The direction of this magnetic field created by the polarized light would be parallel or anti-parallel to the light beam depending on the helicity[6] of the light. Therefore, the circularly polarized light would be able to create the magnetic field at the sample which could be used to switch the sample. The experiments were carried out on a GdFeCo alloy, where the Gd and the FeCo sub-lattices couple anti-ferromagnetically with each other.

The results of their experiments can be seen in Figure 2.2. Here the laser has been swept over a domain wall, so that no pulses overlap. This is done for both a left and a right circularly polarized laser. From this Figure it seems clear that the helicity is important for the switching and thus also the inverse Faraday effect. However, later Ostler *et al.* found that linearly polarized light could also switch the magnetization[20]. They first used atomistic modeling[21] to predict the dynamics of a FeGd alloy after a femtosecond laser pulse. The results of their calculations can be seen in Figure 2.3. Here the blue line represents the magnetization of the Fe, and the red line is the magnetization of the Gd. At $t = 0$, a laser pulse heats the sample and because

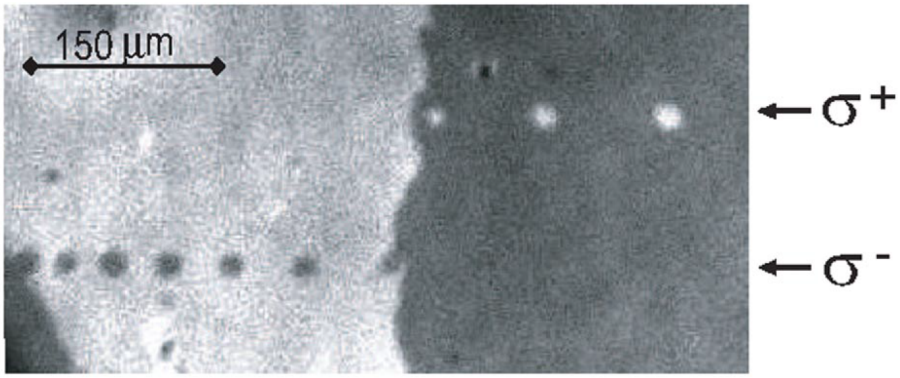

Figure 2.2: Image of a pulsed laser with different helicities swept over a domain wall of a GdFeCo alloy. The image clearly shows that different helicities switch different magnetizations. Figure courtesy of Stanciu *et al.* [6]

of that, both the Fe and the Gd start demagnetizing. The Fe demagnetizes a lot faster and reaches the 0 point before the GD is completely demagnetized. The Gd is then still demagnetizing and due to exchange relaxation, the Fe will cross the 0 magnetization point and remagnetizes in the other direction. The anti-ferromagnetic coupling between the iron and the Gd then causes the Gd to also remagnetize in the opposite direction. When the sample then cools down again, the magnetization of both sublattices will be switched, and so will the magnetization of the alloy. This thus indicated that the heating of the laser was the cause of the switching.

The fact that AOS was a purely thermal effect was then confirmed experimentally as well. In this experiment a GdFeCo alloy similar to that of Stanciu *et al.* was used. The results are shown in Figure 2.4. Single pulses of linearly polarized light were used to switch a homogeneously magnetized sample. Every picture is taken after one laser pulse to show that every pulse switches the magnetization regardless of the initial magnetization of the sample. Multiple other experiments later also confirmed these results[22, 23, 24] and the heating caused by the laser pulse was proved to be the main source of the switching. The reason why the earlier results in Figure 2.2 showed such a discrepancy between right and left circularly polarized light was found to be due to magnetic circular dichroism. This effect causes material with a certain magnetization to absorb more energy from a certain helicity of light. In their case, the GdFeCo with an upwards magnetization absorbed just enough en-

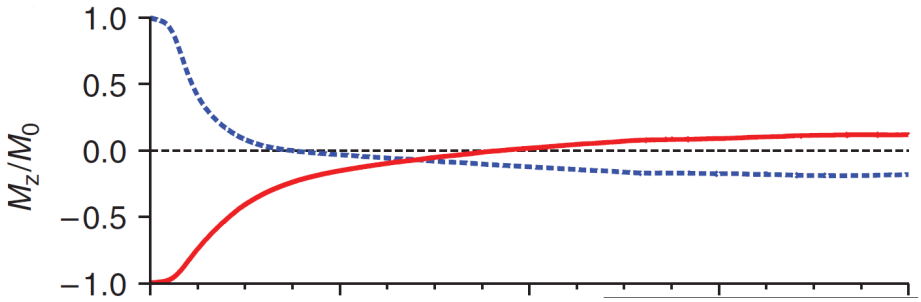

Figure 2.3: Simulated time resolved dynamics of the magnetizatioin of Fe (blue) and Gd (red) after laser pulse excitation by atomistic modeling. Taken from Ostler *et al.*[20]

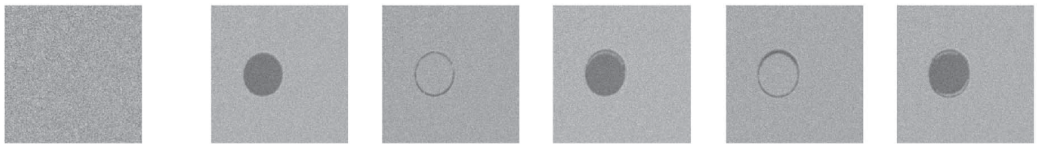

Figure 2.4: Kerr microscope images of a GdFeCo alloy. The alloy starts out homogeneously magnetized in one direction as shown on the left most picture. Then the sample is hit with laser pulses and an image is taken after every pulse. Figure courtesy of Ostler et al.[20]

ergy from the left circularly polarized light beams to switch. From the right circularly polarized light beam however it absorbed less energy and thus did not switch. For the downwards magnetization this effect is exactly opposite, and therefore each helicity of light was only able to switch one magnetization direction [25].

After the discovery of helicity independent single pulse switching, it became clear that this process needed three ingredients. Firstly, an alloy with two magnetic sublattices. These sublattices then have to couple antiferromagnetically and lastly they need to demagnetize at different rates. To verify that these were the needed ingredients, multiple models were introduced. Such models include a general spin dynamic model, models looking at atomistic spins and the microscopic three temperature model, a continuation on the three temperature model that will be elaborated on in the next section. All these models showed that the three aforementioned ingredients were indeed enough to cause all optical magnetic switching. Because these ingredients were now known, the number of materials that could be switched increased rapidly, these included more rare earth - transition metal alloys, but also rare earth free synthetic ferrimagnetic heterostructures[26, 27, 28]. It was even shown that instead of alloys, multilayers could be used such as Co/Gd stacks. The use of multilayers allows for more control over the characteristics of the sample by for example simply changing the thickness of one of the layers, or altering the interface between the layers.

2.4 M3TM

The M3TM is based on the 3TM (three temperature model). The 3TM[5] uses the electron (e), spin (s) and phonon (p) temperatures and heat capacities to create three coupled differential equations. These equations can then be used to calculate the three temperatures, T_e, T_s and T_p. To do this, it does need three coupling constants, G_ep, G_ps and G_es to describe the interaction between the three temperature baths. While this model does allow for a phenomenological description of the magnetization dynamics and can reproduce experimental data, it gives little insight as to what happens on a microscopic scale. In addition, due to the use of coupling constants which are based on experiments, it cannot be used to predict future research on for example different materials.

The M3TM improves on this by explaining the transport of energy to

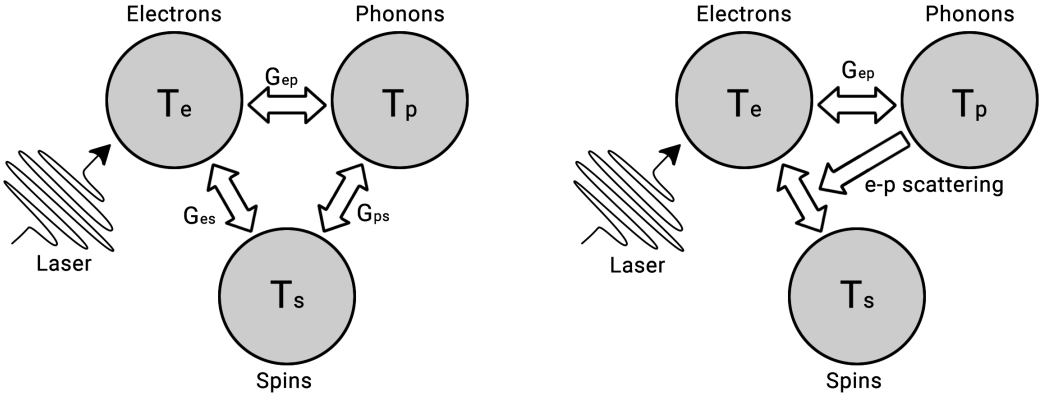

Figure 2.5: On the left the energy transport between the three subsystems according to the 3TM which uses coupling constants to describe the energy flow is shown. On the right the energy transport according to the M3TM model is shown with instead of coupling constants uses e-p scattering and G_{ep}, which is calculated via a microscopic Hamiltonian. Adopted from Dalla Longa[9]

the spin system in a more realistic way. This is done by assuming that the energy and angular momentum transport to and from the spin system happens via electron-phonon scattering events. A schematic which shows the energy transport between the three systems for both the 3TM and the M3TM can be seen in Figure 2.5. The interactions between the subsystems can then be calculated via a combination of 6 Hamiltonians.

$$\mathcal{H} = \mathcal{H}_{\mathrm{e}} + \mathcal{H}_{\mathrm{p}} + \mathcal{H}_{\mathrm{s}} + \mathcal{H}_{\mathrm{ee}} + \mathcal{H}_{\mathrm{ep}} + \mathcal{H}_{\mathrm{eps}}. \tag{2.1}$$

The first Hamiltonian, $\mathcal{H}_{\mathrm{e}}$, is for the electron subsystem. The second Hamiltonian, $\mathcal{H}_{\mathrm{p}}$, is for the phonon subsystem. $\mathcal{H}_{\mathrm{s}}$ is for the spin subsystem. The next Hamiltonians describe the interactions between the subsystems, first is $\mathcal{H}_{\mathrm{ee}}$ which descibes the Coulomb e-e interaction which causes the electron distribution to immediately organize itself according to the electron temperature, T_{e}. There is no interaction Hamiltonian for p-p interactions, since these are assumed to be so fast that the phonons always stay in internal equilibrium. The next term, $\mathcal{H}_{\mathrm{ep}}$, describes the electron phonon scattering. The last term, $\mathcal{H}_{\mathrm{eps}}$ describes the spin flips created by the e-p scattering. This then causes angular momentum to be transported between the spin and the phonon system. These Hamiltonians can the be calculated via Fermi's

golden rule to find the spin dynamics and thus the magnetization dynamics which are as follows[10]:

$$\frac{\mathrm{d}m}{\mathrm{d}t} = R\frac{T_\mathrm{p}}{T_\mathrm{C}}m\left[1 - m\mathrm{coth}\left(m\frac{T_\mathrm{C}}{T_\mathrm{e}}\right)\right]. \tag{2.2}$$

Here m is the normalized magnetization (M/M_s), R is an interaction constant and T_C is the Curie temperature. The M3TM is able to predict many aspects of the measured magnetization dynamics effectively, such as the relaxation times of the electron and phonon temperatures as well as the speed at which magnetization recovers[8]. In addition, the model can be used to predict the dynamics when an external field is applied[9].

2.4.1 Layered M3TM

In order to model the dynamics within stacks instead of alloys, an adapted version of M3TM is used, layered M3TM. The model will be briefly introduced here, but for a more detailed description other papers can be read[2]. In order to model the stack, calculations are made for every layer i. The atoms are structured in an fcc lattice, so every atom has 6 neighbours in its own layer, and 3 neighbouring atoms in layers above and below the atom. The magnetization dynamics caused by e-p scattering do not change much, however spin exchange can happen via e-e scattering between the layers, so that has to be added to equation 2.2. The differential equation for magnetization caused by spin flips from scattering events for layer i will then look as follows.

$$\frac{\mathrm{d}m_\mathrm{i}}{\mathrm{d}t} = R_\mathrm{i}\frac{\Delta_\mathrm{ex,i}}{2k_\mathrm{B}T_\mathrm{C,i}^2}T_\mathrm{p}\left[1 - m_\mathrm{i}\mathrm{coth}\left(m\frac{\Delta_\mathrm{ex,i}}{2k_\mathrm{B}T_\mathrm{e}}\right)\right]. \tag{2.3}$$

Here $\Delta_\mathrm{ex,i}$ is the difference between the energy levels of the spin up and spin down state for the i^th layer. furthermore, the ferromagnetic and antiferromagnetic coupling between the layers will also influence the magnetization dynamics, so some terms have to be added for these interactions as well. The electron and phonon temperatures are assumed to equilibriate throughout the material so quickly, that they are the same within all the layers. Dynamics for these quantities therefore do not change.

3 Methodology

In this chapter the setup as well as the techniques to acquire data and prepare the samples will be explained. First the sputter technique which is used to prepare the samples will be illustrated. Then the principle on which the measurements are based, MOKE, will be explained and afterwards the TR-MOKE setup will be elaborated on. After this, the alignment process of the setup will be shown, as well as some measurements that demonstrate that earlier measurements can be repeated.

3.1 Sputter deposition

In our experiment, multilayer samples with layers of nm thicknesses will be used. To fabricate these samples, a method called magnetron sputter deposition is used. A schematic can be seen in Figure 3.1. The deposition starts by inserting an argon gas into the chamber. Then, a voltage is applied between the target and the anode, which ionizes the argon. The Ar^+ ions are then accelerated towards the target since the target is kept at negative potential. When the Ar^+ ions collide with the target, atoms of the target are knocked off, sputtered, which will then fly to the substrate. Once there, these atoms condense to form a thin film. To increase the deposition rate, a magnet can be placed behind the target to confine the electrons near the target by inducing a rotating motion, increasing the ionization rate of the argon. This increases the sputter rate and thus also the deposition rate. Deposition generally happens at about 0.1 nm/s. Since the samples need to be fabricated at nanometer precision, the process takes place in an ultra-high-vacuum chamber with a pressure of about 10^{-8} mbar. In addition, the substrate is cleaned by acetone and isopropanol in an ultrasound bath.

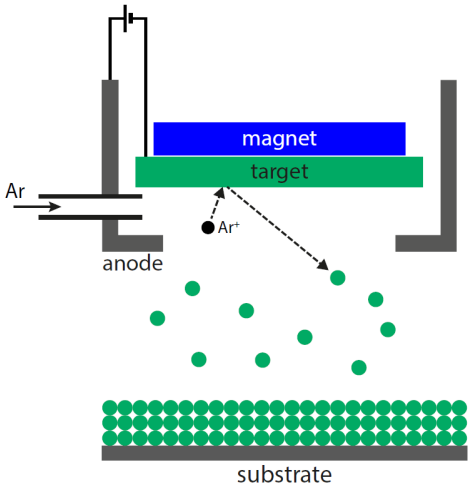

Figure 3.1: Schematic of sputter deposition, adapted from [2]

3.2 MOKE

3.2.1 Background

A magneto optic effect changes the polarization of light when it passes through a material that is magnetized, depending on the magnetization. The first magneto-optic effect that was discovered was the Faraday effect, discovered by Michael Faraday. This effect causes the polarization of an electro-magnetic wave to change when it passes through a material in the presence of a magnetic field [29]. Later, it was discovered by John Kerr that reflection from a magnetic surface also causes a change in the polarization. This effect is called the Magneto Optical Kerr effect[30].

Both MOKE and the Faraday effect stem from the fact that ferromagnetic materials have a dielectric tensor with off-diagonal elements, which causes light with different helicities to experience a different refractive index. Because of this, two different helicities of light will have different amplitudes after reflection due to a difference in absorption, and will be out of phase due to their velocity difference in the material. It should be noted that even reflecting light penetrates some distance within a material, typically 10 - 20 nm for metals[2]. Since every light beam can be seen as a superposition of right and left circularly polarized light, every light beam will experience a

rotation caused by the phase difference of the reflected helicities, and an ellipticity change, caused by the difference in amplitude between the reflected helicities. These differences are called the Kerr rotation θ and the Kerr ellipticity ϵ respectively. The off-diagonal elements of the dielectric tensor that cause these effects are linearly dependent on the magnetization of the material, which means that ϵ and θ are also dependent on the magnetization, and can be used to measure it[31].

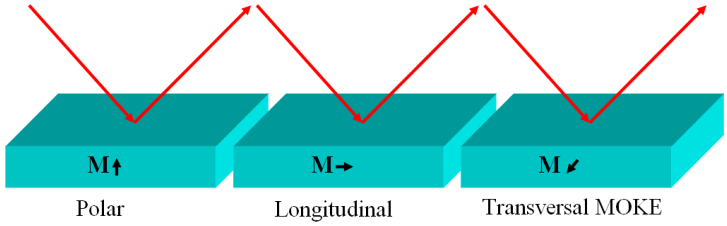

Figure 3.2: Overview of the three MOKE configurations

This measurement can be made via three different configurations, depending on the orientation of the magnetization and the angle between the incoming light beam and the magnetization. The three configurations can be seen Figure 3.2. First is polar MOKE, where the magnetization is out of plane. Next is longitudal MOKE where the magnetization is in plane and parallel to the incoming light beam. The last configuration is transversal MOKE where the magnetization is also in plane, but orthogonal to the incoming light beam. The MOKE signal recieved is highest when the light is parallel to the magnetization direction, so for polar MOKE, the signal is best when the light beam is normal to the sample. In our experiment we are only interested in the out of plane magnetization, and therefore only polar MOKE will be used.

To measure the MOKE signal, the setup shown in Figure 3.3 is used. The light is first linearly polarized, it then passes a photo-elastic modulator (PEM), where the elipticity of the signal is changed as a function of time. It then reflects off the sample and goes through a polarizer and enters the detector.

The reason for introducing the PEM in the system is to increase the signal to noise ratio at the detector. The idea is that the PEM modulates the signal with a certain frequency and this gives a better signal to noise ratio.

The PEM works via the photoelastic effect. This effect causes the birefringence of a material to change depending on the stress on the material.

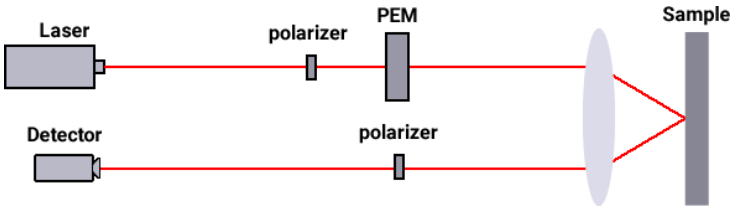

Figure 3.3: Schematic overview of a MOKE measurement setup

Birefringence causes one polarization direction of light to move faster than the other, which can then cause linearly polarized light to become elliptically polarized. Therefore, by applying different stresses to the optical element within the PEM, the ellipticity as well as the rotation of light passing through the PEM can be controlled. To create the modulating effect of the PEM, a current is used to vibrate the optical element which causes it to stretch and thus the birefringence changes. This change in birefringence basically causes the PEM to oscillate between a quarter wave and a half wave plate. The effect of the PEM for light that comes in with a polarization angle of 45 degrees to the fast axis of the PEM can be seen in Figure 3.4. The PEM causes the light to oscillate between left and right polarized light as seen in Figure 3.4 a). This effect does not cause the signal to have a certain periodicity yet as seen in b. However, after reflection with the sample the measured signal will gain a periodicity due to the MOKE. In Figure 3.4 c and d the effect of the Kerr ellipticity can be seen, and in e and f the effect of a Kerr rotation can be seen. The measured signal is calculated thoroughly in other papers [2], but it will have the following form

$$I = A + B\epsilon\cos(\omega t) + C\theta\cos(2\omega t). \tag{3.1}$$

To pick out either the Kerr ellipticity or the Kerr rotation, the lock-in multiplies this signal by a cosine wave of the same frequency and averages over it. Since multiplying cosine waves with different frequencies and averaging over multiple periods causes them to cancel out, only one frequency remains. Therefore, if the lock-in multiplies the signal by a cosine wave with a frequency of ω, only the signal containing the Kerr ellipticity will be left over. In practice however, signals with different frequencies do not simply disappear, but are instead transformed into signals with frequencies depending on the difference between their frequency and that of the lock-in, ω. Therefore, the desired signal will become close to a DC signal and other

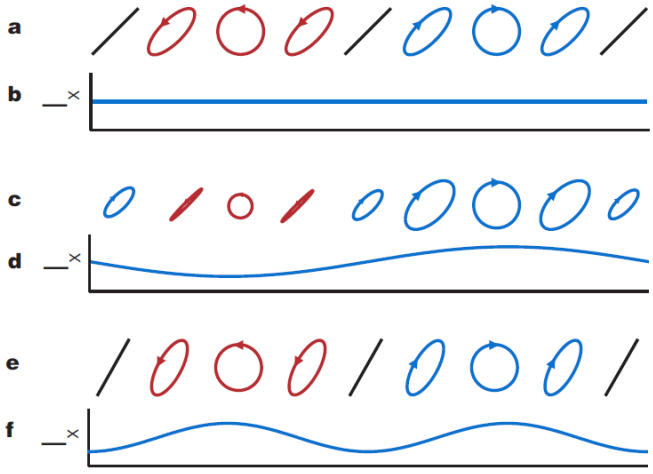

Figure 3.4: Effect of the PEM on the signal. a) shows the effect of the PEM on light with an angle of 45 degrees with the fast axis of the PEM. b) shows the intensity of this light. c) and e) show the effect of the Kerr ellipticity and the Kerr rotation after reflection on the polarization respectively. d) and f) show the effects of the ellipticity and the rotation on the signal strength. Figure courtesy of Schellekens [10]

parts of the signal will have higher frequencies depending on how close their frequency was to ω. Most of the noise can then be filtered out afterwards by a low pass filter, but some noise will always be left in.

3.2.2 TR-MOKE

To create a time-resolved measurement of the magnetization of the sample instead of a static one, a pump probe scheme as shown in Figure 3.5 is used. Here a pulsed laser beam is first split by a beamsplitter into one beam with 90% of the intensity, the pump, and one beam with 10% of the intensity, the probe. The pump is used to excite the sample and in our case switch the sample. The probe is then used to perform the MOKE measurement. Because the probe has such a small intensity it does not affect the magnetization of the sample significantly. The probe has the same path as explained in section 3.2. The pump however first travels through a delay line. This delay line allows for a time difference between when the pump hits the sample and when the probe hits the sample. By measuring the signal of

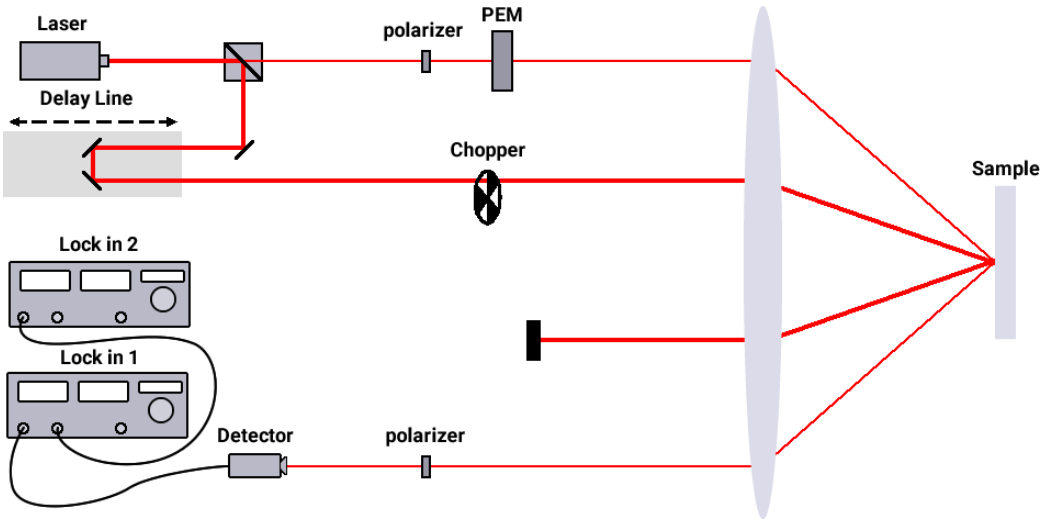

Figure 3.5: Schematic of the Time Resolved MOKE setup

the probe at different time differences, a time resolved measurement can be made. The delay line can travel about 30 centimeters back and forth, which allows for a time difference of 2000 pico seconds.

To increase the signal to noise ratio even further, the pump travels through a chopper before hitting the sample. This creates a second periodicity in the signal. The first periodicity is caused by the PEM as explained in 3.2. Because of the chopper, the measured signal will be oscillating between pumped and un-pumped, and because the frequency of the chopper is lower than that of the PEM, its effect on the signal will still be measurable after the signal has gone through the first lock-in set at the frequency of the PEM. This periodicity can then be exploited by sending the signal from the first lock-in to a second lock-in which is set to the frequency of the chopper. After the pump has hit the sample, its reflection will be blocked so that it cannot affect the measurement.

The expected magnetization of the sample as a function of time can be seen in Figure 3.6 a). Here the moments where the pump hits the sample are shown by the clear switches of the magnetization. With the TR-MOKE setup we can measure the magnetization for a given time delay after the pump has hit the sample. For example at the intervals shown with the blue lines in Figure 3.6 a). However, since the pump switches the magnetization back and forth in the same way, the total measured magnetization will always be zero.

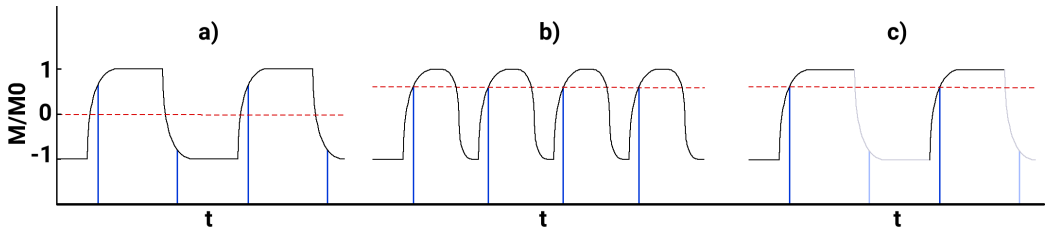

Figure 3.6: Expected sample magnetization measurement, where the expected signal is shown by the dashed red line. In a), the result of measuring every pulse is shown. In b), an external field is applied to cause the magnetization to return to -1 after every pulse. In c), only half of the pulses are measured, which causes the pulses to not cancel each other out.

One way to fix this is to apply an external magnetic field. If we apply a field in the negative magnetization direction, the effect on the magnetization of the sample can be seen in Figure 3.6 b). After every switch, the magnetization now returns to the -1 state because of the field and thus the pump only switches the magnetization one way. The total signal measured will therefore not be 0 as shown by the dashed red line. Using this technique does however mean that we can only measure switching if we apply external fields that are higher than the field required to switch the magnet. To measure the switching without a field, we can instead choose to only register every other probe pulse, which is shown in Figure 3.6 c). This can be done by multiplying the signal with a block function. If the block function then has a period equal to twice the the time between every pulse, only half the pulses will be measured.

3.3 Alignment

All the measurements in this section and the next chapter are done on a Ta(4 nm)/Pt(4 nm)/Co(1 nm)/Gd(3 nm)/Pt(2 nm) sample. The Ta/Pt layer on top is used to stabilize the Co/Gd, and the Pt layer under them is what the sample is grown on. The laser used is a pulse laser with a frequency of 125kHz. Before we can do any relevant measurements, we need to make sure that the pump and the probe are aligned correctly and that the angle between the first polarizer and the PEM allows for relevant magnetization measurements. The first part can be done by scanning the edge of the sample with both the pump and the probe and making sure that they reach the edge

at the same coordinates. Another benefit of this method is that it allows for a way to calculate the FWHM of both the pump and the probe. The FWHM of both the pump and the probe beam after alignment can be found in Table 3.1.

Table 3.1: Pump and probe FWHM for both the y and z direction obtained via edge scans of the sample

	FWHM y (µm)	FWHM z (µm)
Probe	17.5 ± 0.1	19.7 ± 0.1
Pump	92.4 ± 0.1	57.0 ± 0.1

We can see that the pump is a little longer in the y direction, while the probe is slightly elongated in the z direction. The reason for this is because the pump and the probe get focused by a positive lens right before they hit the sample. Because we want the reflections to go in different directions, the pump and probe both enter the lens off center, so that the reflections also exit the lens off center. The probe hits the lens on the right side of the center, while the pump hits the lens above the center. The ellipticity of the pulses is unfortunate, but it should not affect the measurements, since the pump is still at least 3 times as large as the probe in either direction. The probe should be the same size for all the measurements, since the optical path has not been altered, however the pump will be changed.

To check if the probe is aligned correctly and magnetization can be measured, we can make a hysteresis measurement. The magnetization of the sample should be out of plane, so an out of plane external field is applied. The result is shown in Figure 3.7. Here we can see that the sample clearly switches between up and down magnetization at 20 and -20 mT. Another thing to note is that instead of the normal hysteresis loop which would show flat lines when the external field is higher than the coercive field, the magnetization still seems to change. This is due to the fact that the light that measures the magnetization of the sample via the Kerr effect passes through a lens before and after it hits the sample. This lens is also affected by the external magnetic field and becomes magnetized itself. Due to this magnetization, the light experiences a Faraday rotation when it passes through the lens and this rotation is also measured, which causes the slopes at higher external fields seen in Figure 3.7.

To align the pump and the probe even better, we can use a single pump

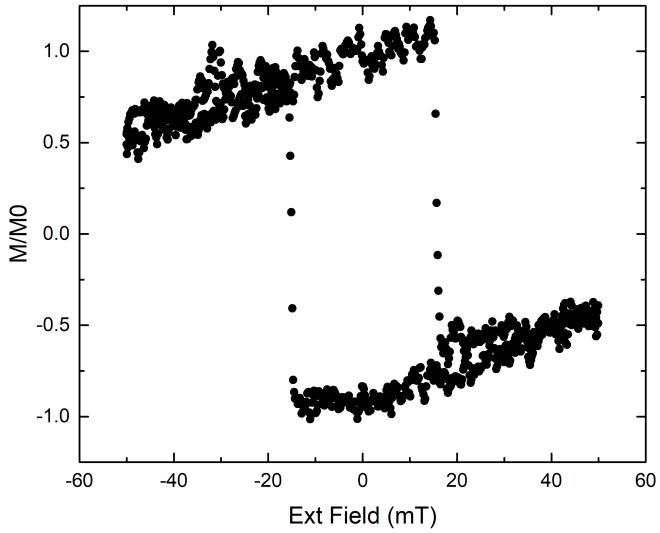

Figure 3.7: Hysteresis loop showing the expected characteristics in adittion to a slight slant due to the Faraday rotation.

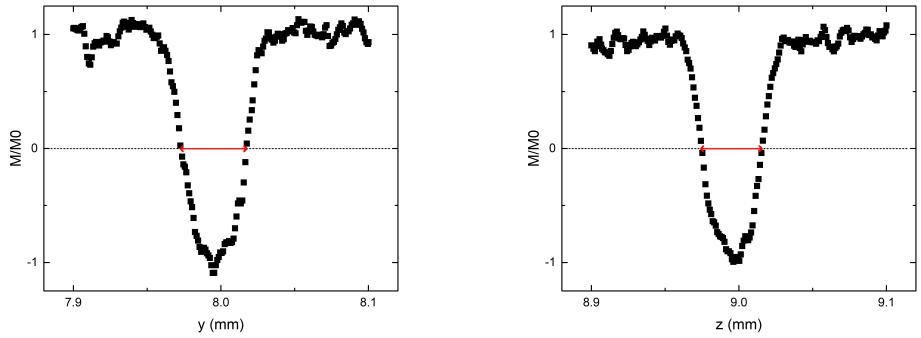

(a) (b)

Figure 3.8: Line scans of the sample after being hit with a single pulse. The red line indicates the switched spot size. A) shows a scan in the y direction, and b) shows a scan in the z direction.

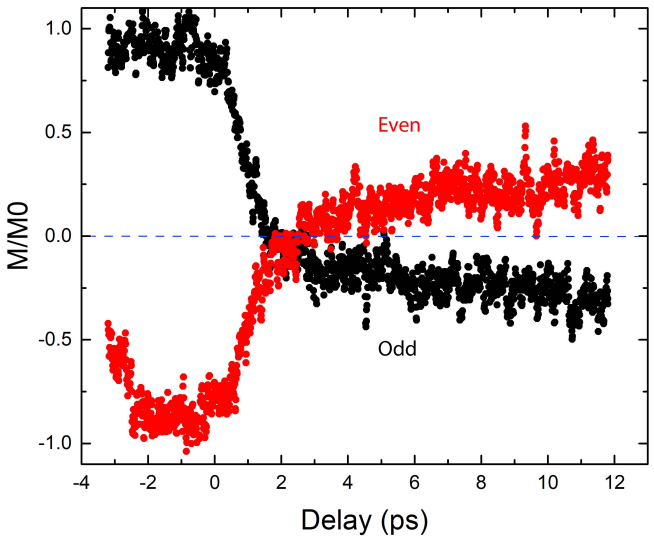

Figure 3.9: Time resolved switch in both directions, normalized by comparing it with a hysteresis loop.

pulse to switch one area of the sample. We can then scan this area with the probe to perfect the alignment as well as to see just how large the switched area is. The results are seen in Figure 3.8, the y and z direction seem to show switched areas of similar sizes, which is a good sign. Every pump pulse has a power of 450 nJ. Which is the maximum laser power that can be achieved.

Since the probe and pump are aligned perfectly and switched spots have been shown, time resolved measurements can be made. This is done by only measuring every other pulse as described in section 3.2.2. Switching in both directions can then be measured without field, which is shown in Figure 3.9. To make sure that the pump switches the sample completely, the signal has to be normalized by comparing it to the hysteresis measurement. This has been done to create Figure 3.9 and it is clear that after every pulse, a full switch happens since the normalized magnetization reaches 1 or -1 depending on which pulse is measured.

Now that switches at zero external field have been measured, time resolved switches at higher external field can also be measured and it can be verified that the expected dynamics are measured. The results are shown in

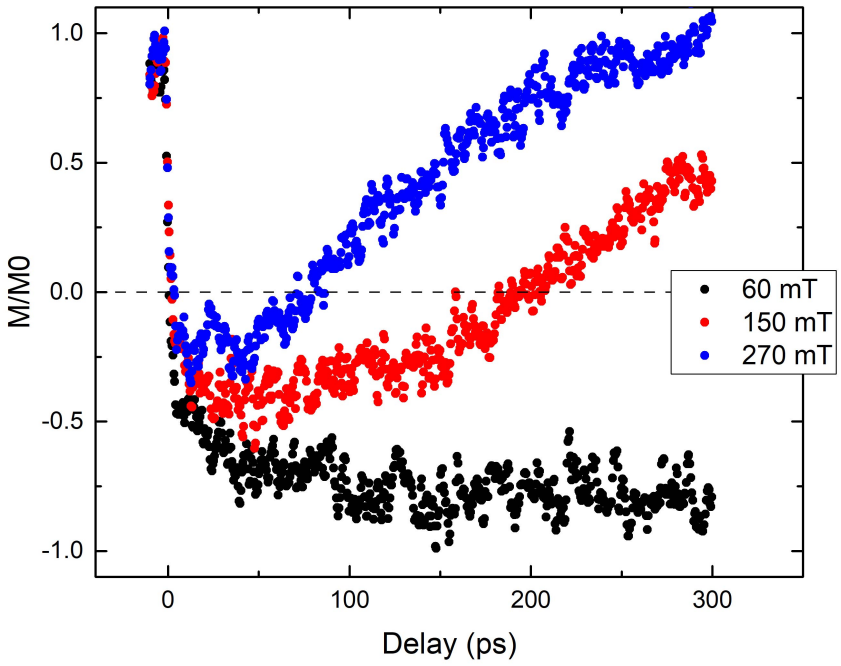

Figure 3.10: Time resolved measurement of the magnetization for different external field strengths

Figure 3.10. The data is normalized in the same way as the switch without field. The results are as expected. Fields below 100 mT really do not change the dynamics of the switching at the measured timescales, while fields above that clearly start pushing the magnetization back to the original level even at short timescales.

4 Results

In this chapter the measurements will be shown and discussed. It starts of by showing the predictions made by the M3TM model for different laser fluences. Then it is shown how the switched spot size can be optimized to allow for measurements at a large laser fluence range. Afterwards this laser fluence range is used to do TR-MOKE measurements with an external field, which can then be compared with the predictions made by the M3TM. Based on the differences between the predictions and the measurements, a modification to the M3TM is proposed.

4.1 M3TM Predictions

It has been shown that for AOS to work, a certain threshold laser fluence is needed. When the fluence is higher than this threshold, the sample will switch, while if it is lower, the sample will only demagnetize. This is also what the M3TM predicts. However, when an external field is applied, the M3TM predicts a new dynamic for high laser fluences, where the sample does not switch anymore. A phase plot for when the sample changes as a function of external field and laser power can be seen in Figure 4.1. This phase plot has been made by simulating 5 Co and 2 Gd layers, the other parameters can be found in the Appendix. The phase plot clearly shows the three regions predicted by the M3TM. The bottom region, c), is where the laser fluence is too low to switch the sample. The middle region, b), is where the laser fluence is high enough to switch the sample. The top region, a), is the new region caused by the external field, which causes the sample to not switch for such high laser fluences. On the right, simulations for the Co magnetization as a function of time can be seen, but the mechanisms that cause these three regions can be better understoodby looking at simulations

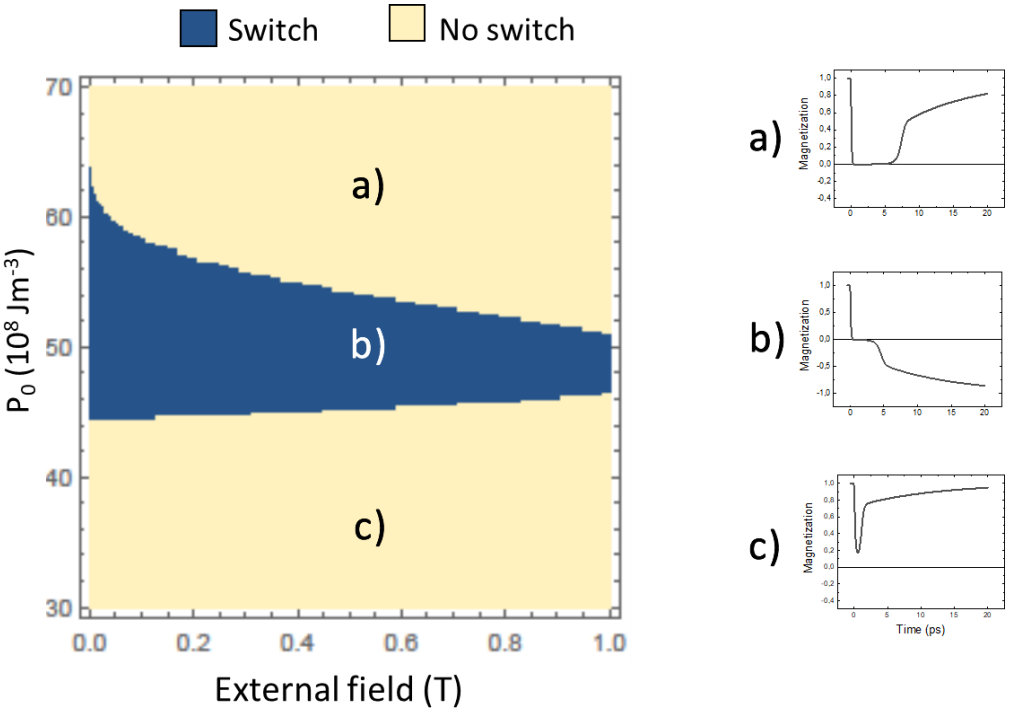

Figure 4.1: Phase plot of laser fluence vs external field that shows when the sample switches. Three different regions can be found in the phase plot, for which time resolved simulations of the Co magnetization are shown on the right. In these simulations the magnetization normalized to that of the Co is shown on the y axis. Figure courtesy of Yannick van Ballegooie [32]

of shorter timescales as shown in Figure 4.2. In Figure 4.2a, the laser power is strong enough to switch the material, and normal switching behaviour can be seen despite the external field. In Figure 4.2b, the laser fluence is so high that switching does not occur anymore. The reason for this is that the sample stays heated for so long, that the Co demagnetizes again after it has crossed the 0 point. When it then cools down afterwards, the Gd is also demagnetized completely and there is no exchange relaxation left to carry the Co magnetization across the 0 magnetization boundary. The external field will then cause the Co to remagnetize in the original direction and no switching has taken place.

It has to be noted that the values on the axes of the phase plot in Figure 4.1 should not be taken too literally, since the M3TM gives qualitative

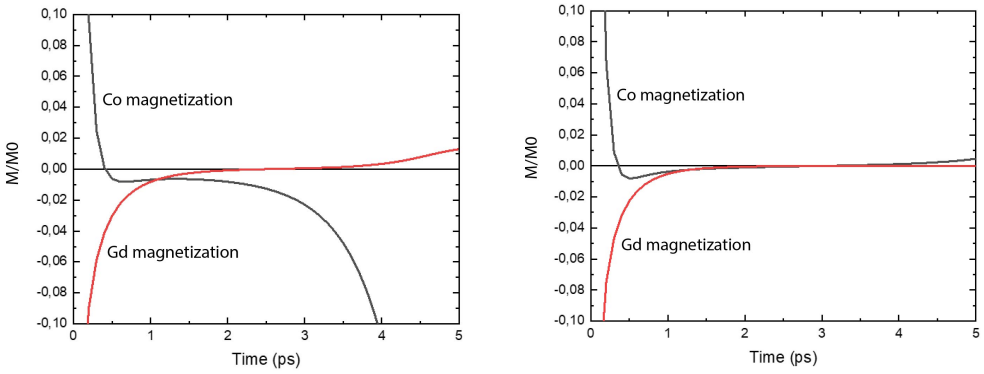

(a) (b)

Figure 4.2: Magnetization dynamics according to the M3TM model with an external field of 0.1 T. In a) the laser fluence is just high enough to switch the material, while in b) the laser fluence is too high which allows the external field to re-magnetize the cobalt in the original direction before switching happens. Figure courtesy of Yannick van Ballegooie [32]

predictions rather than quantitative ones. With that being said, the relative values of the laser power on the y axis are definitely of use. Because of this, it is reasonable to assume if a measurement is made in the bottom part of region b), and thus switching is observed, then by doubling the laser fluence, dynamics from region a) should be measured, and therefore switching should be observed anymore.

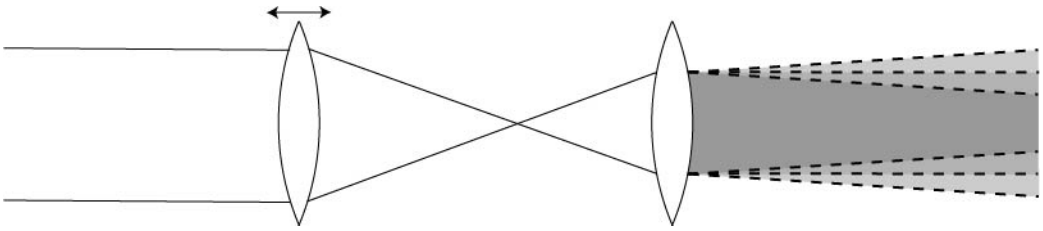

Figure 4.3: Telescope setup consisting of two positive lenses with differing focus lengths. By changing the position of the first lens, the degree to which the beam converges or diverges can be tuned very precisely and this then governs the FWHM of the pump when it hits the sample.

4.2 Switched spot size optimization

To observe the different dynamics predicted by the M3TM, a large laser fluence range for which time resolved switching can be measured is needed. There are two limiting factors here. First off all, the laser has a limiting maximum energy. Secondly, when the laser power is set too low, the switching can not be measured. This is because of the fact that the switched spot becomes smaller when the laser fluence is decreased. At a certain point, this switched spot will therefore be smaller than the probe which is used to measure it and then a clear measurement can not be made anymore. To expand the fluence range, the switched spot size can be maximized by tuning the width of the pump. This is because a large pulse will spread out the energy too much, so that only the center region of the pulse will switch the sample, while a small pulse will switch the entire region hit by the pulse, but this region is still small. There should therefore be an optimum for this spot size. By measuring at this optimum, time resolved switching should be measurable even for low laser fluences.

To focus the probe, a two lens system is used as shown in Figure 4.3. The position of the first lens can be controlled accurately via a translation stage. The distance between the two lenses determines exactly how convergent or divergent the pump is after exiting the second lens, and this in turn controls the size of the FWHM of the pump when it hits the sample. If the lenses are closer, the beam will be less divergent and this will cause the pump to be more in focus when it hits the sample, which results in a smaller FWHM. The FWHM of the probe for different positions of the first lens can be found in Figure 4.4. The FWHMs are measured via edge scans discussed earlier.

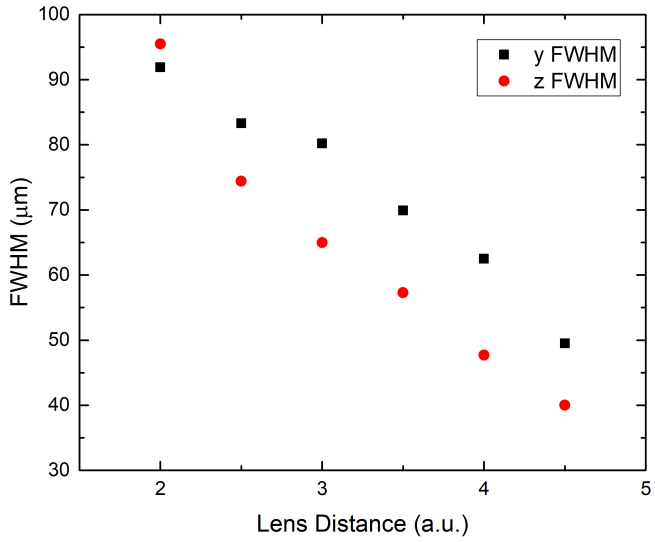

Figure 4.4: FWHM for multiple Lens distances, measured via edge scans

Here a higher Lens Distance means that the lenses are closer to each other. The minimum FWHM that can be reached is 40 μin the z direction. A lower FWHM could be useful for measuring with extremely low laser fluences, however measuring would become difficult due to the fact that the pump and the probe would have almost the same size.

To measure the switched spot size as a function of the distance between the two lenses, a single pump pulse was shot for multiple distances between the two lenses. The width and the height of the switched spots was then measured by looking at line scans as shown in Figure 3.8 and taking the distance between the halfway point on the left of the switched peak and the halfway point on the right. It is assumed here that at this halfway point, the center of the probe is exactly on the edge of the switched area, which would result in a signal with half the magnitude of the full switch. The results can be seen in Figure 4.5. The lens distance has been converted to the FWHM in the y direction by using the data from Figure 4.4. Here the height (z) and with (y) for three laser fluences, 450, 340 and 250 nJ can be seen. Lines have been plotted through the points to show the patterns more clearly. It is clear that the optimization process can really improve the switched spot size.

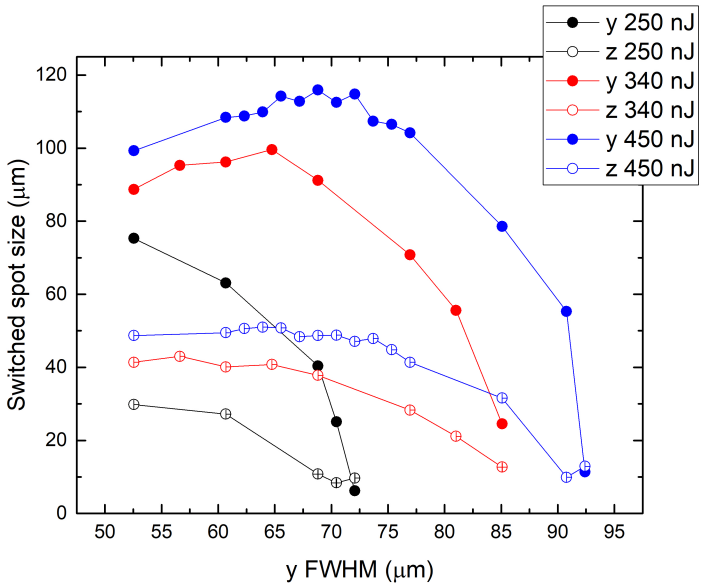

Figure 4.5: Switched spot heights (z) and widths (y) for different laser fluences, 450, 340 and 250 nJ. Lines have been plotted through the points to show the data more clearly.

Table 4.1: Simulated switched spot size at a FWHM of 52.5 μm in the y direction for different laser fluences, with rescaled values based on the measured values.

Laser fluence (nJ)	Switched spot size (μm)	Re-scaled switched spot size (μm)
400	52	70
300	64	86
250	56	75
200	48	65
120	16	22

For a fluence of 250 nJ, the maximum is at a FWHM of 52.5 μm in the y direction or at least very close to this, but lower FWHMs could not be measured. In order to gain the most relevant results for different laser fluences, ranging from 450 nJ to 250 nJ and even lower, the smallest FWHM of 52.5 μm should be used. Here, the pulses with high fluence will still switch a large enough area to measure the effect clearly, while pulses with a low fluence will have their largest reachable switched spot.

To investigate what exactly happens to the spot size of pulses with even lower energy, simulations have been run. To determine the switched spot size, a Gaussian peak with a different FWHM in the y and the z direction has been created and multiplied by the laser fluence to simulate the pump beam energy. This Gaussian is then compared to a threshold fluence of $2.1\text{mJ}/\text{cm}^2$, as measured by Lalieu[2], to find the switched spot size. For the FWHMs of the simulated Gaussian, results from Figure 4.4 have been used. Here it seems that for smaller FWHMs, the difference between the y and the z direction is about 12.5 μm. Therefore the FWHM in the z direction has been taken to be 12.5 μm lower than that in the y direction. The results of a simulation with a laser fluence of 250 nJ can be seen in Figure 4.6. This graph is similar to that of the measurements except for the magnitude of the switched spot size. The value of the simulated switched spot size for multiple laser fluences can be found in Table 4.1. Here the FWHM is set to 52.5 μm in the y direction and 40 μm in the z direction.

Because of the mismatch in magnitude of the switched spot size, an extra column has been added with a re-scaled version of the switched spot size. The re-scaling is done by multiplying all the simulated values by 1.344, the factor by which the measured and the simulated switched spot size at a

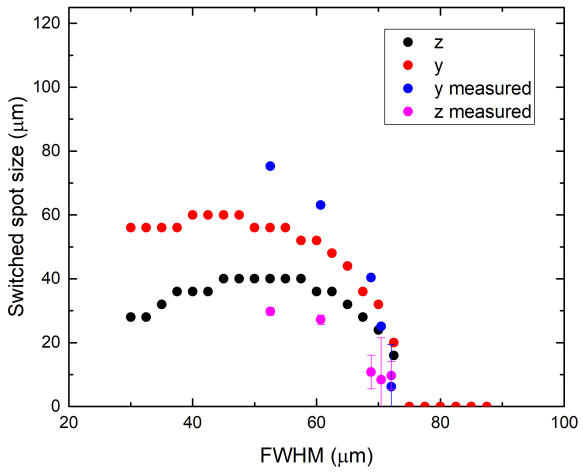

Figure 4.6: Pulsewidth vs y FWHM simulation for a pump fluence of 250nJ with a different y and z FWHM. The measured values have also been plotted to show the similarities

laser fluence of 250 nJ differ. Afterwards, the simulated values match up nicely with the measured ones except for simulated values above 400 nJ. The simulation shows that at low laser fluences, the switched spot size starts to drop quickly. The reason for this is first of all because the maximum of the FWHM vs switched spot size peak moves farther away and secondly because the laser power and thus the switched spot size simply decreases. The rescaled switched spot size at a laser fluence of 120 nJ is 22 μm, which is just bigger than the FWHM of the probe, which means that this is absolutely the lowest laser fluence for which switching can be measured. That being said, since the probe and pump are likely to be misaligned by at least a few microns, it has to be kept in mind that measurements at such low fluences could be flawed.

4.3 Time-resolved switching with external field

The range of powers with which relevant measurements can be done is from 450 nJ to about 120 nJ now, which corresponds to about 6.8 mJ/cm^2 to

1.8 mJ/cm^2. This range is most likely large enough to observe the different regions predicted by the M3TM. The time resolved measurements for an external field of -100 mT at a FWHM in the y direction of 52.5 μm can be found in Figure 4.7. For the lower laser fluences (201 and 241 nJ), the switched spot size is most likely smaller than the FWHM of the probe. This means that the probe measures a combination of switching and demagnetization. For the higher laser fluences, the dynamics look almost the same. The fact that these higher laser fluences show such similar dynamics is unexpected, since the fluence is almost doubled. In addition, since the pump beam has a Gaussian shape, the fluence in the center of the highest pump will be even higher, so different dynamics would definitely be expected for at least part of the switched spot.

Since no different dynamics are measured, there is definitely a mismatch between the measurements and the model. Is is however known that a change from not switching to switching back to not switching is extremely likely, since this is the only current hypothesis that explains the fact that the magnetization starts switching back so quickly when an external field is applied. If the magnetization switched after one pulse within a few 100 pico seconds as measured without field and the field had to reverse the magnetization via domain wall motion, this would take 10 to 40 ns, since the domain walls move only at about 1 micron per nanosecond[33]. The switching mechanism therefore has to be affected by the external field, although the mechanisms in 4.2 a) and b) are unlikely to describe them exactly.

One thing that could be altered about the model is the magnitude of the Gd magnetization. When this is increased, the exchange coupling that causes the Co to switch becomes stronger and thus switching happens more quickly. A simulation of this is shown in Figure 4.8, where the switching is shown for the old Gd magnetization and the new one. Here the power is just strong enough to switch the material ($45{\cdot}10^8$ Jm^{-3}) for the old Gd magnetization. The plateau near the 0 magnetization level is now shorter than it was before, which is already a good sign, since this plateau is not visible in any measurement data. In addition, to create the mechanism shown in Figure 4.2 a), extremely high laser fluences have to be used. A simulation where a power of $65{\cdot}10^8$ Jm^{-3} is used for the altered model is shown in Figure 4.9. With the low Gd magnetization, no switch occurs, while for the higher Gd magnetization, a switch can still be found. The dynamics are however on the cusp of changing to where no switch can be seen. But, to simulate this, simulations of longer timescales have to be done, since higher

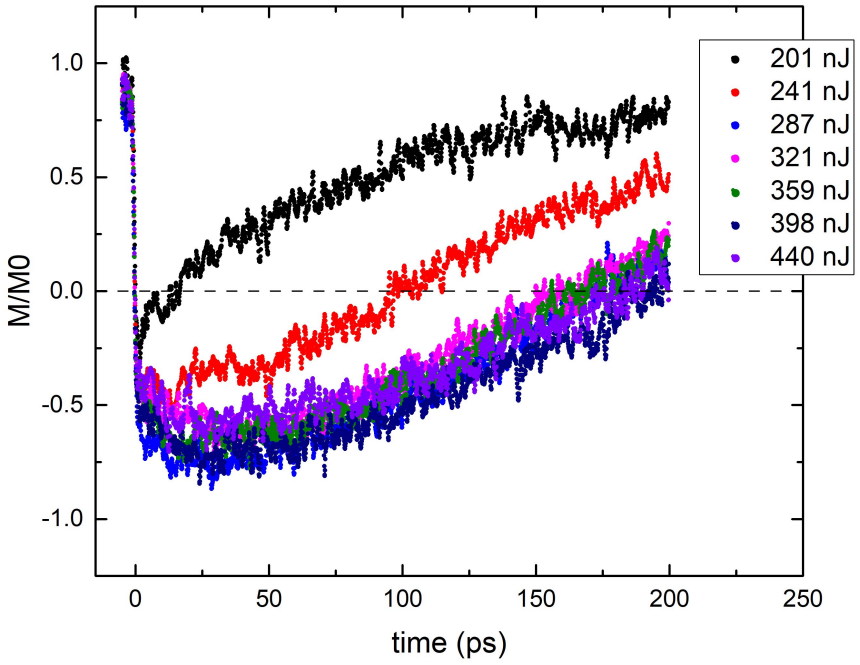

Figure 4.7: TR-MOKE measurements of the sample with an external field of -100 mT for different laser fluences. The low laser fluences show part demagnetization due to the small switched spot size. The higher laser fluences all show the same the same switching dynamics.

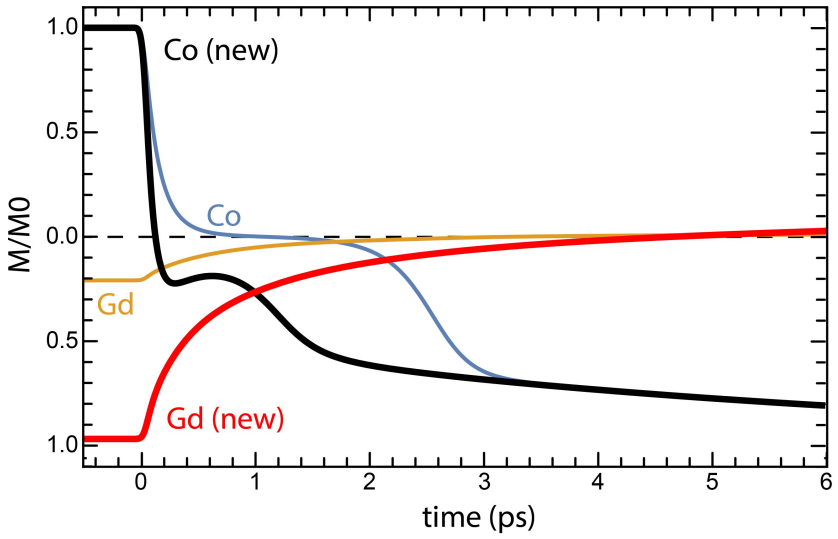

Figure 4.8: Simulated switching dynamics with an external field of 300 mT and a laser fluence of $45{\cdot}10^8$ Jm^{-3}. To realize a higher Gd magnetization, the Curie temperature of Gd has been increased from 292 to 800 K.

fluences only show demagnetization for $t < 6$ ps. This means that the range of fluences for which type b) mechanisms are possible is greatly increased. Instead of going from 45 to $56{\cdot}10^8$ Jm^{-3}, it goes from 35 to at least $65{\cdot}10^8$ Jm^{-3}. This is a reasonable explanation for the similar measurements shown in Figure 4.7. The demagnetization dynamics, type c), do not change when the Gd magnetization is increased, which is good, since these dynamics can be measured for the lower fluences in Figure 4.7.

To realize the strong Gd magnetization, a Curie temperature for Gd has been chosen at 800 K. Another way in which this can be realized is by increasing the ratio of the magnetic moments between Co and Gd, $\frac{\mu_{atCo}}{\mu_{atGd}}$, and slightly increasing the Curie temperature for Gd. These changes to the input parameters are physically hard to argue and since the model is really made to allow for an explanation of the ultra-fast magnetization dynamics on the basis of realistic values, a more realistic way of realizing the increased Gd magnetization is desirable. The understanding of the exact dynamics in the model is however not part of the project and thus more ways of realizing the proposed change of the model have not been found.

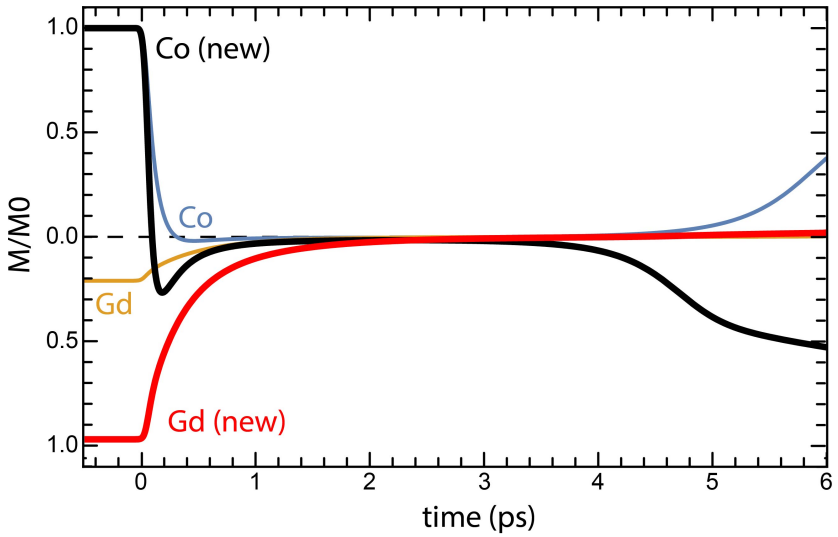

Figure 4.9: Simulated switching dynamics with an external field of 300 mT and a laser fluence of $65{\cdot}10^8$ Jm^{-3}. Here the laser fluence is so high that the old model does not show switching anymore, while the altered model still shows switching.

5 Conclusion

According to the M3TM, different AOS dynamics would be expected if the laser fluence is increased when an external field is present. To observe this, TR-MOKE measurements have been done on a Ta(4 nm)/Pt(4 nm)/Co(1 nm)/Gd(3 nm)/Pt(2 nm) sample with an external field of 100mT, for a fluence range from 120 to 450 nJ. The measurements from 287 to 440 nJ however showed almost exactly the same switching behaviour, while it was expected that the higher fluences should not show switching anymore. There is thus a difference between the M3TM predictions and the measurements. It is possible to get the model more in line with the measurements, by increasing the Gd magnetization relative to that of the Co. By changing the model in this way, the measurements can be explained since this causes the model to predict similar dynamics for a large range of fluences, exactly as observed. To achieve this model change, the Curie temperature of the Gd can be increased to 800K. While this parameter change does allow the model to show all the measured dynamics, the parameter change is not realistic. Therefore this particular change does not make the model more trustworthy in its predictions, even though it would stay consistent with the measurements. A more reasonable way to realize the increased Gd magnetization could possibly be found within the dynamics of the model itself, but finding this requires a much deeper understanding of the model and has thus not been realized.

6 Outlook

While a reasonable proposal has been made for a change in the model and its dynamics, it is still unclear whether this change predicts the dynamics for very high laser fluences accurately. Therefore, the most relevant thing to research is what happens at higher laser fluences. Without improving the laser itself, this can be done in a few different ways. First of all, the FWHM of the pump can be decreased even further, which causes the heating to be more localized and might therefore create strong enough heating of the sample to see different dynamics. Another possibility is to increase the external field. The expectation based on the model is that the dynamics for different laser fluences change more quickly when the external field is higher. This can be seen in Figure 4.2, where the blue area clearly has a downward slope. Even if higher dynamics are not measured for these fields, it is still relevant to look at dynamics for different laser powers for different fields. This is because the model also predicts that there should be a fluence range which is able to switch the sample at low external field, while it will show only demagnetization for higher external fields.

In addition, looking further into the model to find mechanisms that could be altered or added is also interesting. Either to realize a higher Gd magnetization as proposed in this report, or to change something entirely different that is also able to explain the measurements from this report and also those found earlier.

The proposed research ideas should all be able to shed some light onto the edge cases of the M3TM, which is where improvements often can be found. By doing this, the model can be worked out even further and hopefully brought to a state where it can predict more situations accurately, especially concerning the effect of an external field on the switching mechanism.

Bibliography

[1] Ioan Tudosa et al. "The ultimate speed of magnetic switching in granular recording media". In: *Nature* 428 (May 2004), pp. 831–3. DOI: 10.1038/nature02438.

[2] M. Lalieu. "Femtomagnetism meets spintronincs and magnonics". PhD thesis. Eindhoven University of Technology, 2019.

[3] M. Savoini et al. "Highly efficient all-optical switching of magnetization in GdFeCo microstructures by interference-enhanced absorption of light". In: *Phys. Rev. B* 86 (14 Oct. 2012), p. 140404. DOI: 10.1103/PhysRevB.86.140404.

[4] Tom Bostoen, Sape J. Mullender, and Yolande Berbers. "Power-reduction techniques for data-center storage systems". In: *ACM computing surveys* 45.3 (June 2013). eemcs-eprint-24449, p. 33. ISSN: 0360-0300. DOI: 10.1145/2480741.2480750.

[5] E. Beaurepaire et al. "Ultrafast Spin Dynamics in Ferromagnetic Nickel". In: *Phys. Rev. Lett.* 76 (22 May 1996), pp. 4250–4253. DOI: 10.1103/PhysRevLett.76.4250.

[6] C. D. Stanciu et al. "All-Optical Magnetic Recording with Circularly Polarized Light". In: *Phys. Rev. Lett.* 99 (4 July 2007), p. 047601. DOI: 10.1103/PhysRevLett.99.047601.

[7] B. Koopmans et al. "Microscopic model for femtosecond magnetization dynamics". English. In: *Journal of Magnetism and Magnetic Materials* 286 (2005), pp. 271–275. ISSN: 0304-8853. DOI: 10.1016/j.jmmm.2004.09.079.

[8] B. Koopmans et al. "Explaining the paradoxical diversity of ultrafast laser-induced demagnetization". In: *Nature Materials* 9 (Dec. 2009). URL: https://doi.org/10.1038/nmat2593.

[9] F. Dalla Longa. "Laser-induced magnetization dynamics". PhD thesis. Eindhoven University of Technology, 2008.

[10] A. J. Schellekens. "Manipulating spins". PhD thesis. Eindhoven University of Technology, 2014.

[11] Johannes Kimling et al. "Ultrafast demagnetization of FePt:Cu thin films and the role of magnetic heat capacity". In: *Phys. Rev. B* 90 (22 Dec. 2014), p. 224408. DOI: 10.1103/PhysRevB.90.224408.

[12] Richard P. Feynmann, Robert Leighton, and Matthew Sands. *The Feynman Lectures on Physics*. Vol. 2. Addison-Wesley, 1963. Chap. 37.

[13] R. J. D. Tilley. *Understanding Solids*. John Wiley and Sons, 2004, p. 368.

[14] A. V. Zaitsev. "Quasiclassical equations of the theory of superconductivity for contiguous metals and the properties of constricted microcontacts". In: *Zh. Eksp. Teor. Fiz* 86 (1984), pp. 1742–1758.

[15] A. Vaterlaus et al. "Different spin and lattice temperatures observed by spin-polarized photoemission with picosecond laser pulses". In: *Journal of Applied Physics* 67.9 (1990), pp. 5661–5663. DOI: 10.1063/1.345918. eprint: https://doi.org/10.1063/1.345918.

[16] J. Hohlfeld et al. "Nonequilibrium Magnetization Dynamics of Nickel". In: *Phys. Rev. Lett.* 78 (25 June 1997), pp. 4861–4864. DOI: 10.1103/PhysRevLett.78.4861.

[17] J. Güdde et al. "Magnetization dynamics of Ni and Co films on Cu(001) and of bulk nickel surfaces". In: *Phys. Rev. B* 59 (10 Mar. 1999), R6608–R6611. DOI: 10.1103/PhysRevB.59.R6608.

[18] B. Koopmans et al. "Ultrafast Magneto-Optics in Nickel: Magnetism or Optics?" In: *Physical review letters* 85 (Aug. 2000), pp. 844–7. DOI: 10.1103/PhysRevLett.85.844.

[19] "Electric Forces in a Transparent Dispersive Medium". In: *JETP* 12.5 (July 1960), p. 1008.

[20] T. A. Ostler et al. "Ultrafast heating as a sufficient stimulus for magnetization reversal in a ferrimagnet". In: *Nature Commun* (2012), p. 666.

[21] J.K. Chen, D.Y. Tzou, and J.E. Beraun. "A semiclassical two-temperature model for ultrafast laser heating". In: *International Journal of Heat and Mass Transfer* 49 (Jan. 2006), pp. 307–316. DOI: 10.1016/j.ijheatmasstransfer.2005.06.022.

[22] J. H. Mentink et al. "Ultrafast Spin Dynamics in Multisublattice Magnets". In: *Phys. Rev. Lett.* 108 (5 Jan. 2012), p. 057202. DOI: 10.1103/PhysRevLett.108.057202.

[23] A. J. Schellekens and B. Koopmans. "Microscopic model for ultrafast magnetization dynamics of multisublattice magnets". In: *Phys. Rev. B* 87 (2 Jan. 2013), p. 020407. DOI: 10.1103/PhysRevB.87.020407.

[24] S. Gerlach et al. "Modeling ultrafast all-optical switching in synthetic ferrimagnets". In: *Phys. Rev. B* 95 (22 June 2017), p. 224435. DOI: 10.1103/PhysRevB.95.224435.

[25] A. R. Khorsand et al. "Role of Magnetic Circular Dichroism in All-Optical Magnetic Recording". In: *Phys. Rev. Lett.* 108 (12 Mar. 2012), p. 127205. DOI: 10.1103/PhysRevLett.108.127205.

[26] S. Alebrand et al. "Light-induced magnetization reversal of high-anisotropy TbCo alloy films". In: *Appl. Phys. Lett.* 101 (16 2012). DOI: 10.1063/1.4759109.

[27] S. Mangin et al. *Engineered materials for all-optical helicity-dependent magnetic switching*. Feb. 2014. URL: https://doi.org/10.1038/nmat3864.

[28] A. Hassdenteufel et al. "Dependence of all-optical magnetic switching on the sublattice magnetization orientation in Tb-Fe thin films". In: *2015 IEEE International Magnetics Conference (INTERMAG)* (May 2015), pp. 1–1. ISSN: 2150-4598. DOI: 10.1109/INTMAG.2015.7157030.

[29] M. Faraday. *On the magnetization of light and the illumination of magnetic lines of force*. The Royal Society, 1846.

[30] John Kerr LL.D. "On rotation of the plane of polarization by reflection from the pole of a magnet". In: *The London, Edinburgh, and Dublin Philosophical Magazine and Journal of Science* 3.19 (1877), pp. 321–343. DOI: 10.1080/14786447708639245.

[31] J. L. Erskine and E. A. Stern. "Magneto-optic Kerr Effect in Ni, Co, and Fe". In: *Phys. Rev. Lett.* 30 (26 June 1973), pp. 1329–1332. DOI: 10.1103/PhysRevLett.30.1329.

[32] Y. van Ballegooie. *2019-04-16 Yannick van Ballegooie Update Master 2*. Eindhoven University of Technology.

[33] R. Hertel and C. Andreas. *Magnetic Nano- and Microwires*. 2015, pp. 653, 677. URL: https://doi.org/10.1016/B978-0-08-100164-6.00022-9.

7 Appendix

7.1 Standard M3TM parameters

In Table 7.1 the parameters for the M3TM simulations can be found. These paramaters have been used to create Figures 4.1 and 4.2, as well as Figures 4.8 and 4.9 where for the T_c Gd has been changed to 292 for the new simulations. Most of these values come from measurements, while some are based on assumptions.

Table 7.1: Standard parameters for the M3TM simulations

T_{c} Co	1388 K
a_{sf} Co	0.15
r_{at} Co	2.7 Å
μ_{at} Co	1.72 J/T
T_c Gd	292 K
a_{sf} Gd	0.08
r_{at} Gd	2.37 Å
μ_{at} Gd	7.55 J/T
$\tau_{\mathrm{heat\ \ diffusion}}$	10 ps
$J_{\mathrm{ex}}/k_{\mathrm{B}}$	-600 K/J
$Exch.rate\ Co/Gd$	$2.5{\cdot}10^{-9}$/s
T_{amb}	295